

Article

Investigation of Surface Nanoclusters and Paramagnetic Centers of ZnO/Por-Si Structures as the Basis of Sensory Properties

Danatbek Murzalinov ^{1,*}, Tatyana Seredavina ¹, Ainagul Kemelbekova ¹, Yulia Spivak ², Vyacheslav Moshnikov ², Daniya Mukhamedshina ¹, Kostantin Mit' ¹, Nurzhan Ussipov ³, Elena Dmitriyeva ¹, Sultan Zhantuarov ¹, Sayora Ibraimova ¹, Kazybek Aimaganbetov ¹, Ekaterina Bondar ¹ and Anastasiya Fedosimova ¹

- ¹ Institute of Physics and Technology, Satbayev University, Almaty 050013, Kazakhstan; t.seredavina@sci.kz (T.S.); kemelbekova@sci.kz (A.K.); d.mukhamedshina@sci.kz (D.M.); k.mit@sci.kz (K.M.); dmitriyeva@sci.kz (E.D.); s.zhantuarov@sci.kz (S.Z.); ibraimova@sci.kz (S.I.); k.aimaganbetov@sci.kz (K.A.); bondar@sci.kz (E.B.); a.fedosimova@sci.kz (A.F.)
- ² Microelectronics Department, Saint-Petersburg State Electrotechnical University, Professora Popova Street, 197376 Saint-Petersburg, Russia; ymospivak@etu.ru (Y.S.); vamoshnikov@etu.ru (V.M.)
- ³ Department of Solid State Physics and Nonlinear Physics, Al-Farabi Kazakh National University, Almaty 050040, Kazakhstan; ussipov.nurzhan@kaznu.kz
- * Correspondence: murzalinov@sci.kz

Abstract: The detection of particles with uncompensated charge and the determination of the features of their interaction during the formation of nanocrystals on substrates with a developed surface are an interesting area of research. The porous surface formed via the electrochemical etching of silicon acquired fractal properties as a result of the deposition of zinc oxide layers. Microscopy methods using different resolutions revealed a hierarchical structure of the surface, where each of the three consecutive levels contains uniformly distributed formations. The deposition of 20 layers of ZnO maximizes the concentration of nanocrystals at the pore boundaries, while the deposition of 25 layers leads to the formation of a continuous layer. The increase in photoluminescence intensity with an increase in the number of deposited layers is due to the saturation of surface nanostructures with electrons through several mechanisms. Electron paramagnetic resonance (EPR) studies have shown that the main mechanism of radiation recombination is the capture of electrons on oxygen vacancies. The different nature of the EPR saturation of the signal of interconnected paramagnetic centers revealed the formation of zinc oxide particles at the boundaries of pores with different sizes. The results of these studies of surface-active structures effectively complement the knowledge about sensory materials.

Keywords: electrochemical etching; levels of porosity; ZnO coating deposition; light-emitting clusters; photoluminescence; electron paramagnetic resonance; saturation of structures with electrons; saturation of the EPR signal; oxygen vacancies; capture of electrons



Citation: Murzalinov, D.; Seredavina, T.; Kemelbekova, A.; Spivak, Y.; Moshnikov, V.; Mukhamedshina, D.; Mit', K.; Ussipov, N.; Dmitriyeva, E.; Zhantuarov, S.; et al. Investigation of Surface Nanoclusters and Paramagnetic Centers of ZnO/Por-Si Structures as the Basis of Sensory Properties. *Processes* **2023**, *11*, 3332. <https://doi.org/10.3390/pr11123332>

Academic Editor: Wei Chen

Received: 28 October 2023

Revised: 25 November 2023

Accepted: 28 November 2023

Published: 30 November 2023



Copyright: © 2023 by the authors. Licensee MDPI, Basel, Switzerland. This article is an open access article distributed under the terms and conditions of the Creative Commons Attribution (CC BY) license (<https://creativecommons.org/licenses/by/4.0/>).

1. Introduction

One of the most important trends in modern materials science is the transition from traditional methods of obtaining layered and film nanostructures to an active atomic-molecular design combining several hierarchical levels [1–4]. Such structures, due to synergetic effects and developed interfaces, will have new unique properties.

The traditional approach to controlling the properties of semiconductor materials is based on the use of doping processes with impurities that create certain electronic levels in the band gap. However, in some cases, the traditional approach is associated with fundamental limitations due to the absence of impurities with suitable properties, the low

limit of solubility of atoms of many impurities in the semiconductor crystal lattice, the high concentration of electrically active intrinsic lattice defects in the doped material, etc. In this regard, in recent years, a new approach to managing the properties of semiconductors has been actively developing, based on the formation of nanoscale clusters in the semiconductor matrix, which may include atoms of introduced impurities and atoms of their own components, as well as their own point defects of the crystal lattice [5].

Due to the small size of the cluster, the electron wave function is limited by a potential barrier in all three directions and clusters can create local levels similar to impurity levels in the band gap of the semiconductor. Obviously, the formation of a suitable set of cluster levels in a semiconductor is a difficult task. Nevertheless, the use of clusters is necessary when there are no impurities in nature that could create the required electronic level in a semiconductor, or when the solubility of impurities is too small. The complex structure of clusters provides many opportunities for the construction of electronic levels.

If clusters are the main part of the material, then changes in their size and concentration lead to changes in the fundamental properties of the semiconductor, such as the band gap width, the amount of conductivity, the energy of fundamental optical transitions, etc. This opens up opportunities for the design of new semiconductor materials, the properties of which may differ significantly from the properties manifested by the same semiconductor in monocrystalline or amorphous states [5].

An example of a cluster material is porous silicon (Por-Si), which, in comparison with monocrystalline Si, has a more effective photoluminescence (PL). This material is obtained via the electrochemical processing of crystalline Si plates, as a result of which, the structure of nanoscale clusters and filaments is formed.

The structure of the porous silicon film can be controlled by the current density and concentration of chemical reagents in the electrochemical reaction, doping and pretreatment of the initial plate [5].

The control of the technological conditions for the synthesis of porous silicon and the choice of parameters of the initial material allows for obtaining Por-Si in a wide range of porosity values (from 5–6% to 90–95%), specific surface area (60–800 m²/g), pore diameters (micro-, meso-macropores) and their hierarchical levels. Thus, porous silicon actually represents a class of materials that differ significantly in properties (electrophysical, luminescent, adsorption, heat conducting, mechanical, gas and liquid permeability, etc.) [1].

Based on the variety of properties of the resulting porous silicon, it is possible to create devices for various purposes. Sensors based on Por-Si are promising types of devices [6–8]. Obviously, this is due to the process of electrochemical etching of silicon, which leads to the intensive formation of clusters, with a high concentration of particles with broken bonds on their surfaces. A change in the material's resistance, the measure of sensitivity, is related to this process. Based on this, different types of sensors can be obtained, in particular photosensitive ones.

It is known that with a decrease in the size of silicon nanocrystallites, the radiation energy of Por-Si increases in the entire visible spectrum of photoluminescence. Deposition of thin films of ZnO on porous silicon substrates makes it possible to significantly expand the radiation spectrum. Studies of photoluminescence of a ZnO/Por-Si nanocomposite excited by a He Cd laser with an energy of 3.81 eV that confirms the presence of peaks of red (1.69 eV), green (2.34 eV) and blue (2.88 eV) radiation in the spectrum with high intensity in the range from 1.4 to 3.3 eV [9].

Nanoscale zinc oxide has many different configurations, and therefore, it can be classified as a novel material with a wide range of potential applications. Zinc oxide can be in the form of one, two and three-dimensional structures. The largest group consists of one-dimensional structures, which include nanorods [10–12], needles [13], helices, springs, and rings [14], ribbons [15], tubes [16–18], combs, belts [19] and wires [20–22]. Two-dimensional (2D) structures can be in the form of a nanoplate/nanosheet, and nano pellets can be obtained (synthesized) from zinc oxide [23,24]. Three-dimensional structures of zinc oxide include snowflakes, flowers, dandelions, coniferous urchin-like structures, etc. [25–28].

Therefore, ZnO has one of the largest assortments of different particle structures among all known materials [29].

The variety of zinc oxide nanostructures determines the advantages of devices based on them. Due to lower cost and easier etching, ZnO is considered as an ideal alternative material for the production of flat-panel displays, compared to ITO [29]. The response of the sensor based on ZnO/Por-Si is faster than that based on SnO₂/Por-Si. This is due to the higher sensitivity and increased surface area of ZnO/Por-Si nanostructures [30].

Photoluminescence and photosensitivity of zinc oxide may be associated with the transfer of charges from the conduction band and valence band to oxygen vacancies with their subsequent ionization. Such a formation of zinc oxide particles can have a wide range of properties depending on the local spatial orientation. In particular, there may be an isotropic or anisotropic interaction between the paramagnetic particles. On the other hand, the resulting field depends on the types of particles and the number of neighboring atoms. These factors lead to the formation of unique types of surface structures, which affects the individual characteristics of the EPR spectra.

With an increase in the concentration of oxygen vacancies, the width of the ZnO band gap decreases. This is due to the formation of additional levels in the band gap when charges are captured on oxygen vacancies. This leads to a broadening of the conduction and valence bands and, consequently, to an increase in the absorption of visible light [31].

The formation of a developed structure of the ZnO surface under nonequilibrium conditions of deposition of a substance via spray pyrolysis is associated with the formation of a large number of vacancies [32]. The determination of the features of the interaction of vacancies leads to an understanding of the process of defect formation of matter.

Statement of the problem: Deposition of zinc oxide layers on the Por-Si surface leads to a reduction in the pore size, which increases the sensitivity of the material. The nucleation of structures occurs mainly at the boundaries of the pores, so the size of the crystals forming depends on the size of the pores. However, it is difficult to distinguish the processes of formation of nanocrystallites at the boundaries of pores with different sizes.

Using microscopy methods, it is possible to detect the distribution of nanocrystals on the sample surface. However, it will be necessary to repeatedly take images, while there is a high probability that the surface will not be fully explored. EPR studies, with a sequential increase in the microwave power, could effectively complement the description of this parameter.

Reducing the sensitivity of sensor materials as a result of degradation is an urgent problem. The saturation of the EPR signal makes it possible to determine the energy stability of the formed structures.

Novelty: the application of the effects of saturation of the microwave power makes it possible to manifest signals of various defects and features of their behavior associated with localization at the boundaries of pores of different sizes.

Goal: investigation of the synthesis of ZnO particles on a porous-hierarchical surface, as well as their distribution and energy stability, which affect the sensitivity of ZnO/Por-Si structures.

The importance of this work is as follows:

As a result of the deposition of zinc oxide layers on Por-Si, a fractal structure with several hierarchical levels of porosity on the surface was formed.

The study of the transformation of a complex EPR signal by changing the registration conditions made it possible to identify its components based on the difference in growth under the influence of microwave power.

As a result of the formation of a homogeneous coating at the pore boundaries when depositing 25 layers of ZnO, a significant increase in photoluminescence was achieved, probably associated with saturation of the surface structures with charges.

To compare the methods used in this and other works, the following analysis was carried out. In [33], Por-Si substrates were obtained by electrochemical anodizing of n-type crystalline silicon with a resistivity from 1 to 10 ohms·cm and an orientation of 100. The

deposition of ZnO on the surface of porous silicon was carried out using a carbothermic reaction at constant Ar and O₂ flow rates. The reduced exciton radiation is explained by non-radiative transitions associated with the capture of charges on vacancy traps. The consequence of this is the depletion of carriers in nanostructures. It is noticeable that the EPR spectrum for these samples has a complex structure and there is an overlap of signals. Probably, if, in addition to the work carried out, the spectra were also recorded with other signal registration parameters (change in microwave power, modulation amplitude, gain factor), the characteristics of the signals would manifest more clearly and their relationship with the structure would be clearer.

In [34], hybrid nanostructures based on ZnO films deposited on macroporous silicon substrates using the sol-gel spin coating and ultrasonic spray pyrolysis techniques were obtained. In order to check the quality of the ZnO films, the transmittance was measured in the range 350–750 nm. Measurements have shown that the average optical transparency of ZnO films exceeds 84% in the visible range, and there is noticeable gain in the region of 360 nm and 370 nm. The sharp ultraviolet absorption edges of the samples at a wavelength close to 360–370 nm corresponds to the intrinsic bandgap energy of ZnO due to the presence of energy levels associated with defects [35,36]. The nature of such sensitivity to light could be revealed by a more detailed study of the structure of ZnO defects and the features of their interaction using the EPR method.

The effect of the passivating layer of zinc oxide thin films on porous silicon with low (18%) and high (80%) porosity was investigated in [37]. After ZnO coating on the Por-Si etched for 420 min, the relative intensity of 3.2 eV UV PL emission bands increased by a factor of 14.5. The study of Fourier infrared spectroscopy additionally confirms the formation of a surface oxide layer (1000–1300 cm⁻¹) and associated defects on Por-Si, as well as on Por-Si coated with ZnO. The creation of an optoelectronic device with high luminescent properties should ensure the formation of structures with energetically stable properties, but such an analysis has not been carried out. And also from the AFM microscopy section, the mechanism of formation of ZnO structures on the Por-Si surface, which determines the size of the obtained zinc oxide particles, is not clear.

2. Materials and Methods

2.1. Materials and Synthesis

2.1.1. Synthesis of Porous Silicon

The Por-Si layers were obtained via electrochemical anodic etching of monocrystalline silicon in an electrolyte based on an aqueous solution of hydrogen fluoride with the addition of isopropyl alcohol.

Monocrystalline silicon of the mark KEF-4.5 (n-Si (111) with a resistivity of 4.5 Ω cm, doping impurity—P), was used as the initial material. Before electrochemical etching, all silicon wafers were cleaned by exposure in acetone, isopropyl alcohol and distilled water in an ultrasonic bath (UZ Sapphire). The following reagents were used for the electrolyte: hydrogen fluoride 45.00%, GOST 10484-78, CAS: 7664-39-3; isopropyl alcohol SSPIRT-9805.F01080, GOST 9805-84, CAS: 67-63-0; distilled water.

Electrochemical etching of Si was carried out in a single-chamber electrochemical cell. A glass-carbon crucible was used as an electrochemical bath, which served as an electrode—cathode, and was also chemically resistant to the composition of the electrolyte. Electrochemical etching was carried out in galvanostatic mode.

After electrochemical etching, porous silicon samples were washed in isopropyl alcohol and distilled water. It was shown that a micro-mesoporous skin layer of complex composition can form on the surface of macroporous silicon. To remove this layer the samples were chemically kept in a 20% aqueous solution of hydrogen fluoride for 1–2 min. After obtaining Por-Si and removing the surface layer, the samples were immediately used for the synthesis of ZnO.

2.1.2. Features of the Formation of Porous Silicon When the Anodizing Current Density Changes

The anodizing current density (J_A) is one of the main technological parameters for obtaining Por-Si via electrochemical etching of silicon. It changed from 40 mA/cm² to 80 mA/cm² within 10 min. In work [1], it was found that at high values of the J_A in Si (111) and the direction of the current lines perpendicular to the plane of the plate surface, the formation of pore channels occurs not only in the directions of the easiest etching but also along the current lines, representing the result of competing processes. At low anodizing current densities, the direction of the pore channels is determined by the substrate, while a Por-Si layer with a “tree” type structure is formed. When a certain threshold value of the current density is exceeded, the direction of propagation of the pore channels predominantly coincides with the direction of the electric field lines. This effect has a significant practical application in the formation of rod structures in Si (111) [38]. The combination of conditions, $J_A > J_{A \text{ threshold}} = 70 \text{ mA/cm}^2$, and orientation of the electrodes of the plane-parallel surface of the silicon wafer allowed us to achieve the formation of vertical pore channels in the same way as in work [38]. Such structures will have a larger specific surface area compared to silicon nanorods obtained using traditional MACE technology [39] and are promising for the development of hybrid gas sensors based on them [40].

2.1.3. Synthesis and Deposition of a ZnO Coating on a Substrate Sol–Gel Method

The film-forming solution was synthesized using the sol–gel technique. The use of this method is due to the simplicity of implementation and the possibility of effective influence on the processes of growth of structures. The sol solution was produced by mixing 0.1 M zinc acetate dihydrate ($\text{Zn}(\text{CH}_3\text{COO})_2 \cdot 2\text{H}_2\text{O}$) with 9 mL isopropanol ($\text{C}_3\text{H}_7\text{OH}$) as a solvent and 1 mL monoethanolamine ($\text{C}_2\text{H}_7\text{NO}$) as a stabilizing agent. Within an hour of the synthesis of the solutions, ZnO films started to be deposited on the substrate.

The nucleation conditions of ZnO particles are crucial parameters for the synthesis of structures with stable properties. This is especially important if the process takes place on a developed surface, where the growth of structures on the walls of the pore channels is possible. This process carried out using spin-coating method when the table rotates at a speed of ~3400 rpm, for 1 min. In this way, only such a layer was formed on the surface, which was held by the forces of surface tension, and the excess solution was removed. Further, the samples were dried at 130 °C and then annealed at 450 °C (1 h) to obtain stable nuclei of the substance.

Deposition of the Film Layers

Substrates on the heating element were sprayed with liquid solutions using a pneumatic airbrush. The distance between the airbrush nozzle and the substrates ranged between 20 and 30 cm. The spray solution flow was most consistent when the pressure was adjusted to 1.4 bar.

The substrate's temperature ranged from 350 to 400 °C. At this temperature, the solvent evaporated before the aerosol droplets were deposited on the surface. In this case, zinc oxide films with spherical and hexagonal cell structure were obtained. The deposition of 20 and 25 layers of ZnO is due to the formation of the thinnest layers, in the photoluminescence spectrum of which there are characteristic peaks for zinc oxide.

2.2. Characterization Methods

The structure of the deposited films was studied using X-ray diffraction by applying a highly collimated (0.05×1.5) mm² of a monochromatic ($\text{CuK}\alpha$) X-ray beam directed at an angle of 5° to the surface of the sample. The intensity of X-ray reflections along the debyeagram was measured every $2\theta = 0.05^\circ$ on the microdensitometer (MD-100, Carl Zeu's,

Germany). The average size of the crystallites was calculated from the half-width of the X-ray lines using the Jones method.

Scanning electron microscope (SEM) (JSM-6490LA (“JEOL”, Akishima, Japan). The take-off angle for the JSM-6490LA is 35°, with an analytical working distance of 10 mm. The microscope has a high resolution of 3.0 nm.

EPR spectrometer “JEOL” (JES-FA200, Akishima, Japan). Measurements in the ranges ~9.4 GHz (X-Band) and ~35 GHz (Q-Band). Microwave frequency stability ~ 10⁻⁶. Sensitivity—7 × 10⁹/10⁻⁴ Tl. Resolution—2.35 μT. Output power—from 200 mW to 0.1 μW, quality factor (Q-factor) 18,000.

The study of the nature of the EPR signal saturation took place under identical conditions with a change in the power of microwave radiation in the range from 1 to 12 mW for the sample with 20 layers (m = 5.2 mg) of ZnO and from 1 to 7.6 mW for the sample with 25 layers (m = 7.4 mg).

Atomic force microscope (AFM) (Japan, “JEOL” JSPM-5200). The vacuum depth is up to 10⁻⁶ mm Hg. Scanning mode (AFM AC), scanning speed of the entire image is 13 min, brands of probes applied (NSC35/AIBS). Scan scale varied as follows—10 × 10 μm, 20 × 20 μm, 50 × 50 nm, 143 × 143 nm.

The spectrophotometer Cary Eclipse (Agilent, Santa Clara, CA, USA) was used to detect photoluminescence from 200 to 800 nm. The spectral width of the slit in this device is changeable, ranging from 0.5 to 2.4 nm. As a radiation source, a tungsten-halogen lamp was used for visible measurements and a deuterium lamp was used for UV measurements.

2.3. Methodology for Determining the Fractal Properties of the Surface of Samples

A number of methods, including «Box-counting» and «Brownian motion» [41] are employed to determine the fractal dimensions of images. The simplest and widely used technique is «Box counting» [42–46]. This method involves creating a grid of square cells with a given side length δ that cover parts of the image and then counting the number of cells $N(\delta)$. If the image has fractal behavior, then the relationship between $N(\delta)$ and δ is given by the following equation:

$$N(\delta) \sim \delta^{-D} \quad (1)$$

where D is the fractal dimension of the image. The logarithmic transformation of this law allows us to obtain a linear dependence and a graph with a slope of $-D$. Thus, the dimension of fractality can be estimated by the gradient of the graph $\ln N(\delta)$ relative to $\ln \delta$, given by the following expression:

$$D = -\lim_{\delta \rightarrow 0} \frac{\ln N(\delta)}{\ln \delta} \quad (2)$$

This expression is a good way to quantify the degree of complexity and heterogeneity of the image structure.

3. Results

3.1. Investigation of Surface Morphology via Scanning Electron Microscopy

To study the processes of formation of the surface structure, SEM images of the initial sample and with a ZnO coating were obtained. The macroporous structure of the surface of the samples is clearly represented in the images at a magnification of 430 times (Figure 1).

The deposition of ZnO layers on porous silicon led to a decrease in the diameter of the macropores (Figure 1b,c).

Figure 2 shows the results of the SEM study with a higher resolution. The images show surface structures with a step-like nature of porosity, from macro- to micro-dimensional. It is also possible to determine the developed structure of the pore walls.

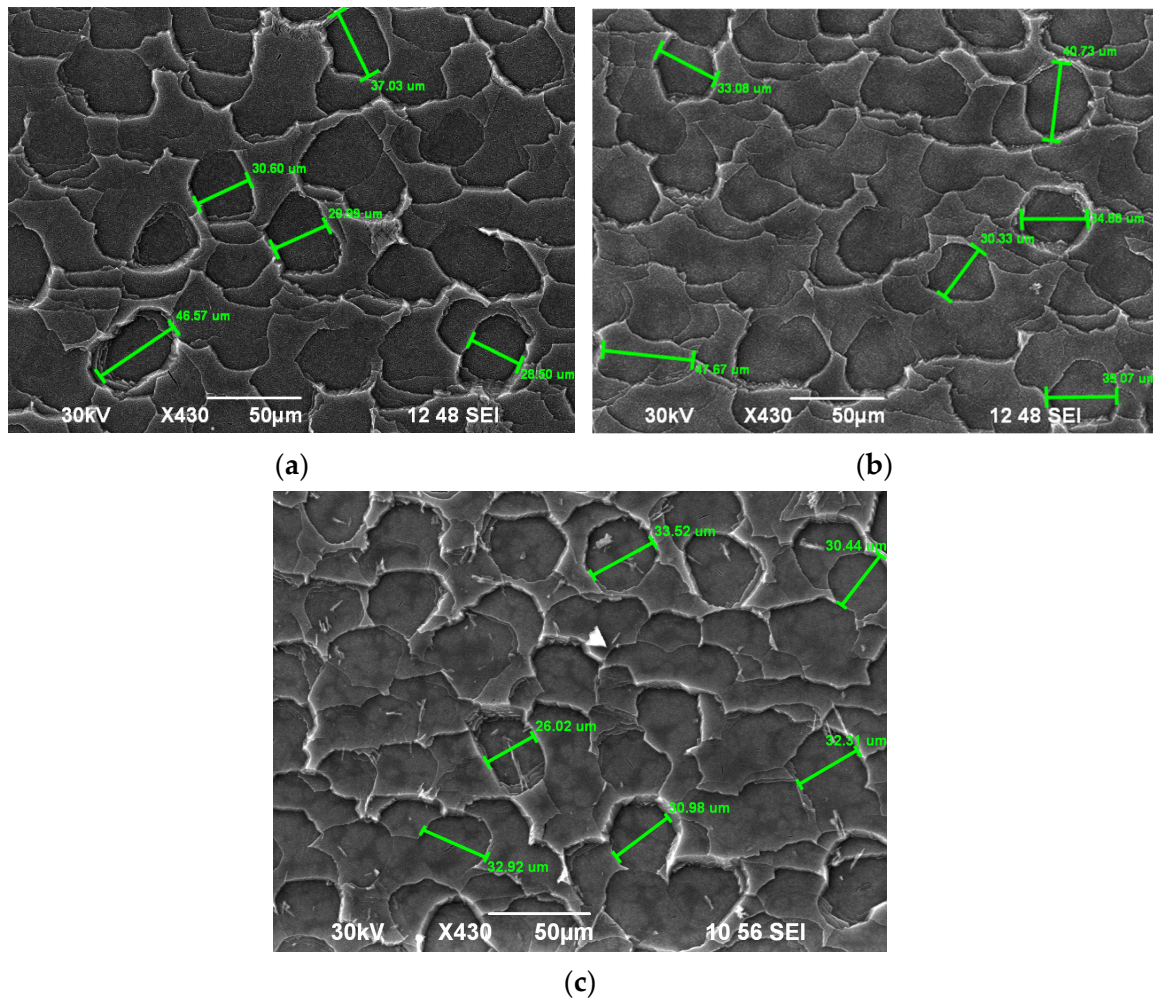


Figure 1. SEM images of samples at magnification in $\times 430$: (a) without ZnO coating; (b) porous silicon with 20 layers of ZnO; (c) porous silicon with 25 layers of ZnO.

The deposition of ZnO layers took place in an air atmosphere, and therefore, in addition to zinc oxide, a thin layer of SiO_2 was formed. The multilayer structure increases the mechanical strength of the samples and forms effective light-emitting particles.

The deposition of 20 layers of coating leads to the formation of the most developed structure of the pore boundaries by the formation of individual crystallites (Figure 2c). Such structures contain a large number of micro- and nanoscale grains containing particles with broken bonds. A further increase in the number of layers to 25 forms a smoother surface of the macropore boundaries through the formation of a continuous layer (Figure 3a).

The dynamics of changes in the morphology of the surface of samples with an increase in the scale of $\times 430$ and $\times 11,000$ are presented in Table 1.

Table 1. Dynamics of changes in the morphology of the surface of samples as a result of the formation of ZnO layers on the surface of Por-Si.

	Pore Size Range, μm ($\times 430$)	Pore Size Range, nm ($\times 11,000$)
uncoated	25–50	600–800
20 layers of coating	30–45	520–705
25 layers of coating	25–34	350–500

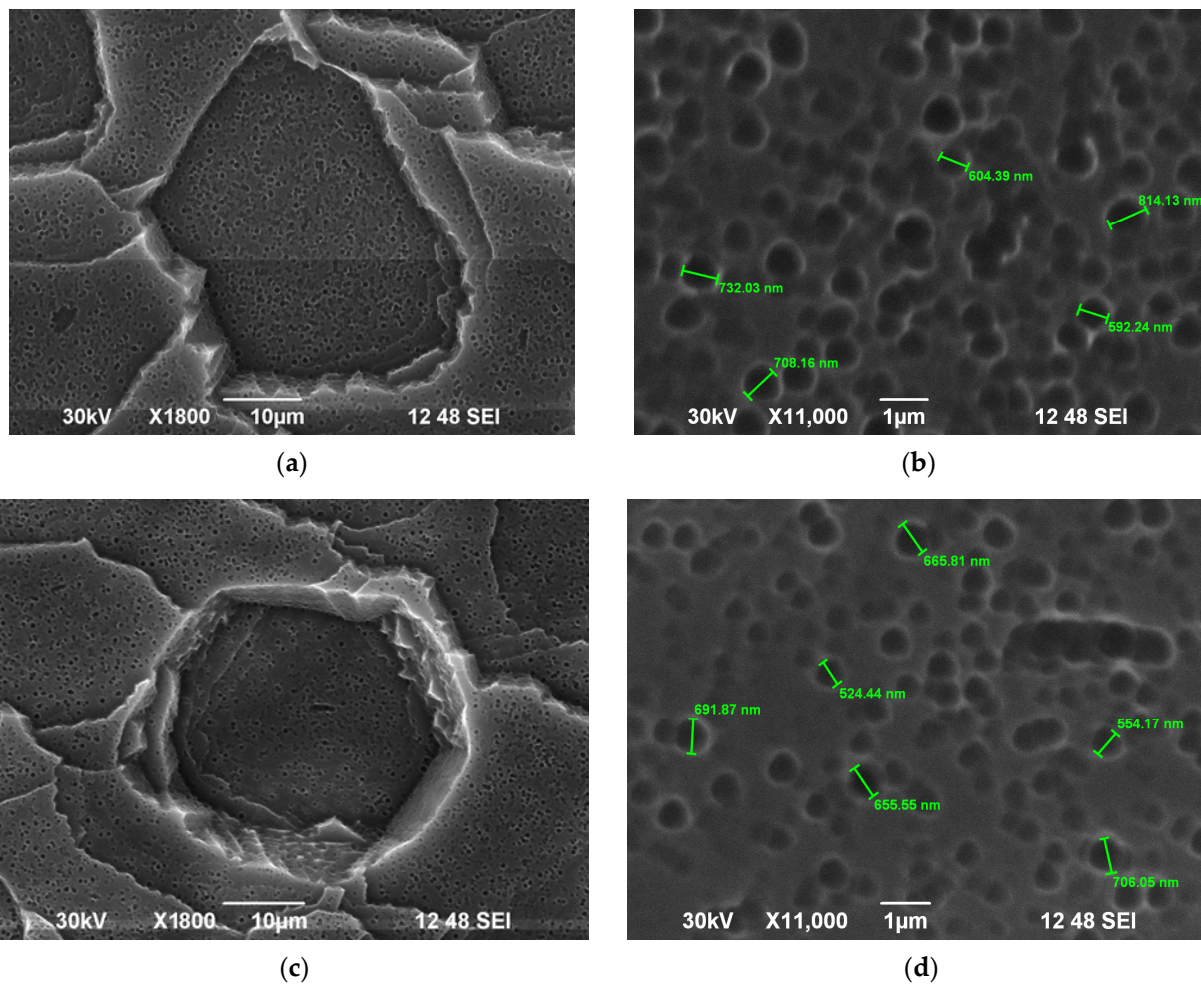


Figure 2. SEM images of samples: (a) without ZnO coating at $\times 1800$ magnification; (b) without ZnO coating at $\times 11,000$ magnification; (c) porous silicon with 20 layers of ZnO at $\times 1800$ magnification; (d) porous silicon with 20 layers of ZnO at $\times 11,000$ magnification.

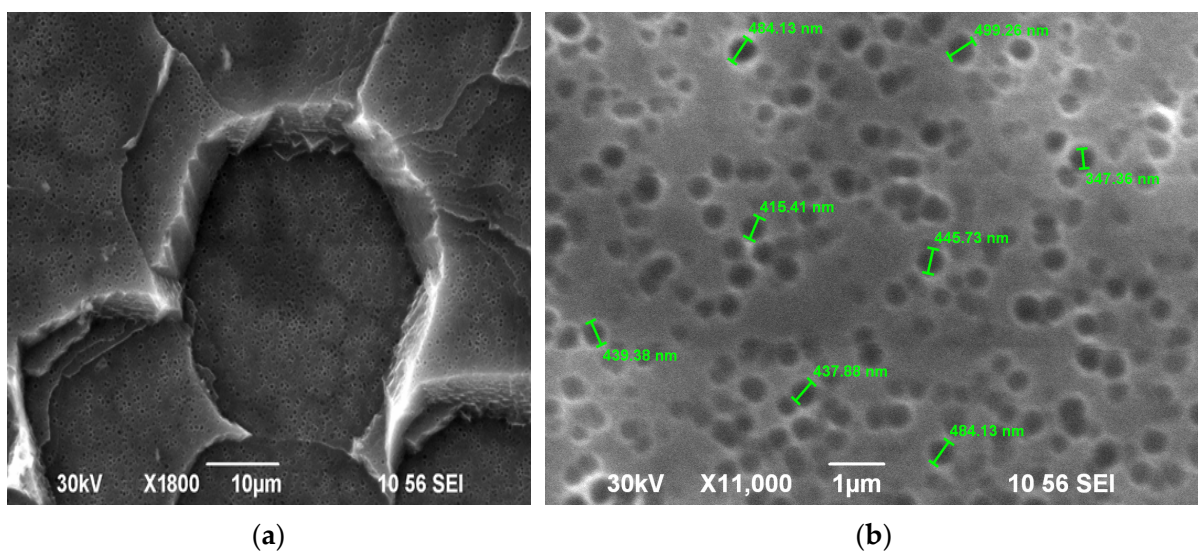


Figure 3. SEM images of samples: (a) porous silicon with 25 layers of ZnO at $\times 1800$ magnification; (b) porous silicon with 25 layers of ZnO at $\times 11,000$ magnification.

The localization of the coating occurs mainly at the boundaries of the pores, which is associated with a high concentration of particles with an uncompensated charge on them. Thus, with an increase in the number of layers, the surface becomes more finely porous, and the porosity is more uniform in size. In this case, a hierarchical surface with signs of fractality is formed.

3.2. Investigations of the Fractal Properties of the Sample Surface

The principle of structural hierarchy means the following: structures of one type are modules, “building blocks”, from which structures of the second level are formed, having significantly larger spatial dimensions, and structures of the second level, in turn, are combined into structures of the third level, etc. This leads to the fact that the modules, connecting to the structure, transfer to it part of their functions, the degrees of freedom [47]. An important aspect of fractal structures is their dimension invariance when the scale changes.

The formed Por-Si layers have a regularity of surface morphology when considering different levels of hierarchy. At the same time, the deposition of ZnO makes a significant contribution to the formation of a more uniform structure in size. To determine the invariance of structures when changing the scale of the surface, the following analysis was carried out.

Before calculating the fractal dimension, a threshold value of pixel intensity was determined, which was used to select the appropriate structural elements in the image. This stage is important because different thresholds allow us to pay attention to different levels of details and textures. To carry this out, a histogram of the pixel intensity in the black-and-white image was obtained in Figure 4b, which represents the distribution of intensities from low to high values. The threshold value was selected based on the histogram analysis and can be interpreted as a transition point between the background and the objects (macropores) in the image.

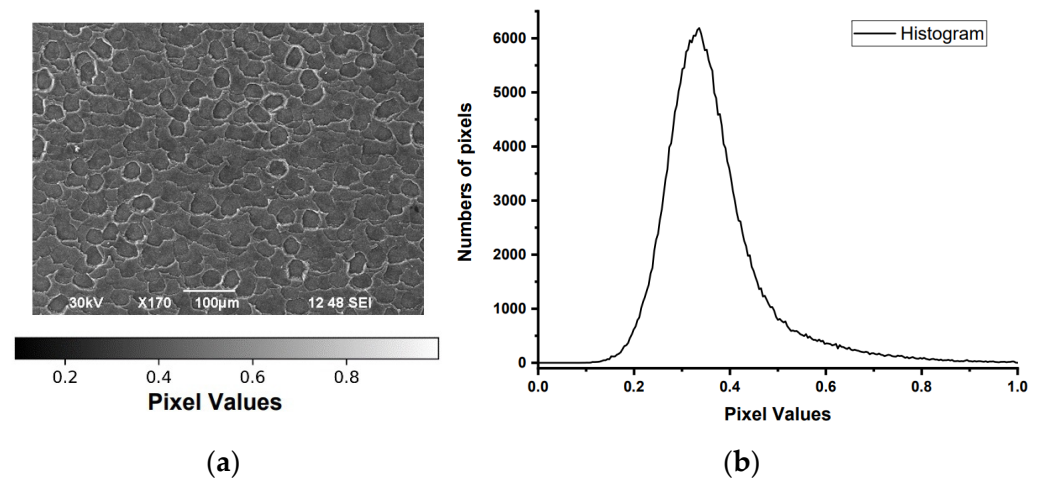


Figure 4. (a) SEM image with a scale of 100 μm for a sample without depositing ZnO layers and a scale of pixel intensity values. (b) Histogram of the sample image with a coating of 20 layers, scale 100 μm.

It can be seen from the histogram of the image that the number of pixels reaches a maximum intensity at 0.4, which we then select as a threshold. Next, those pixels whose intensity exceeds this threshold were highlighted. Thus, a subset of pixels was created, which represent the structures we are interested in. Further, this subset was used to estimate the fractal dimension (Figure 5).

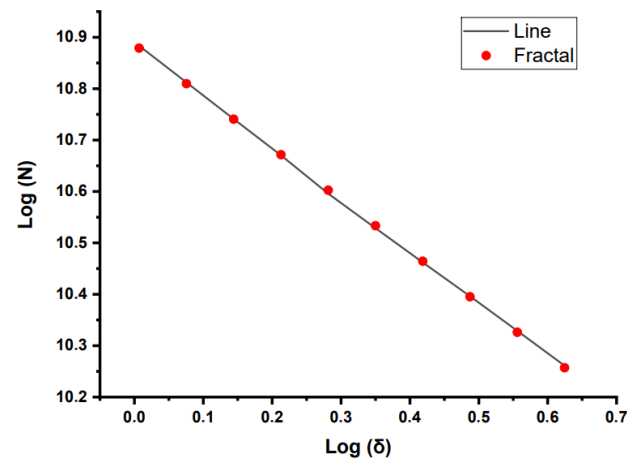


Figure 5. Dependence of the logarithm of the number of cells $N(\delta)$ on the scale δ .

The resulting graph demonstrates a linear relationship. With a threshold value of pixel intensity equal to 0.4, the fractal dimension of the image of a sample coated with 20 layers at the scale 100 nm was $D = 1$.

Further, in order to confirm the presence of fractality for a sample with 20 coating layers, a study was conducted at various pixel intensity thresholds. Figure 6 shows the results of this comparative analysis for image scales of 100 μm and 50 μm .

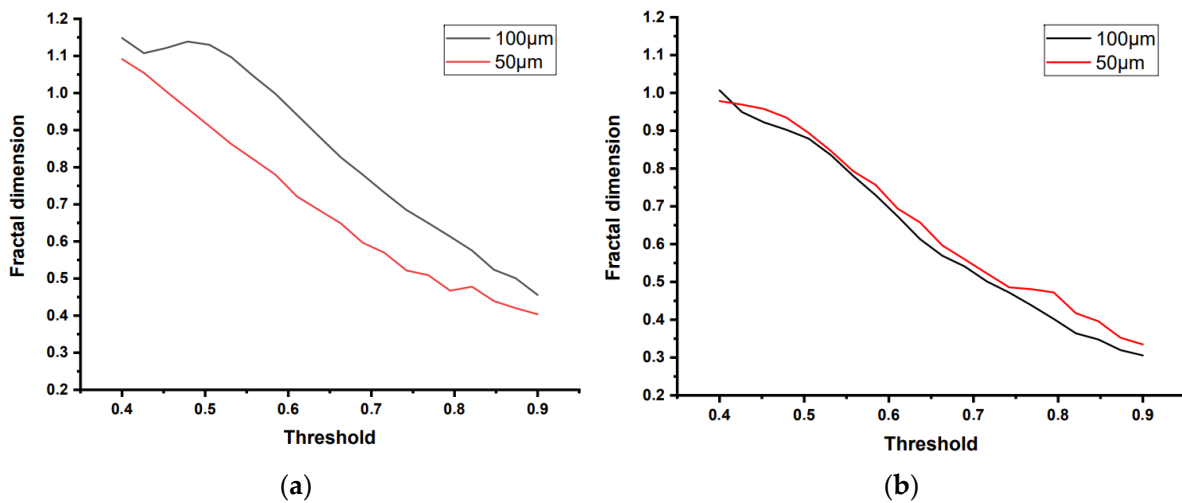


Figure 6. The dependence of the fractal dimension on changes in the threshold values of pixel intensity: (a) without coating; (b) with the deposition of 20 layers of zinc oxide.

Changing the intensity of pixels leads to the selection of various details and features of the structure, which is reflected in a change in the fractal dimension. In Figure 6a, there is a noticeable change in the dimension of the structure when the scale changes, for a sample without coating. This indicates that the object does not have a fractal nature. In contrast to this, the sample with a deposition of 20 layers of coating, when changing the scale, allowed us to preserve the dimension of the structure (Figure 6b). This is due to the presence of fractal properties in this structure. Small fluctuations in the value of the fractal dimension are associated with the noise factor.

A fractal surface structure was also observed for a sample with 25 layers of zinc oxide, which is described in the next section.

3.3. Investigation of Surface Morphology Using Atomic Force Microscopy

For a detailed study of the structures inside the macropores of a sample with 25 layers of ZnO, the atomic force microscopy was applied. Figure 7a,b show the uniform distribution of micropores on the surface, and between them, clusters of matter are formed.

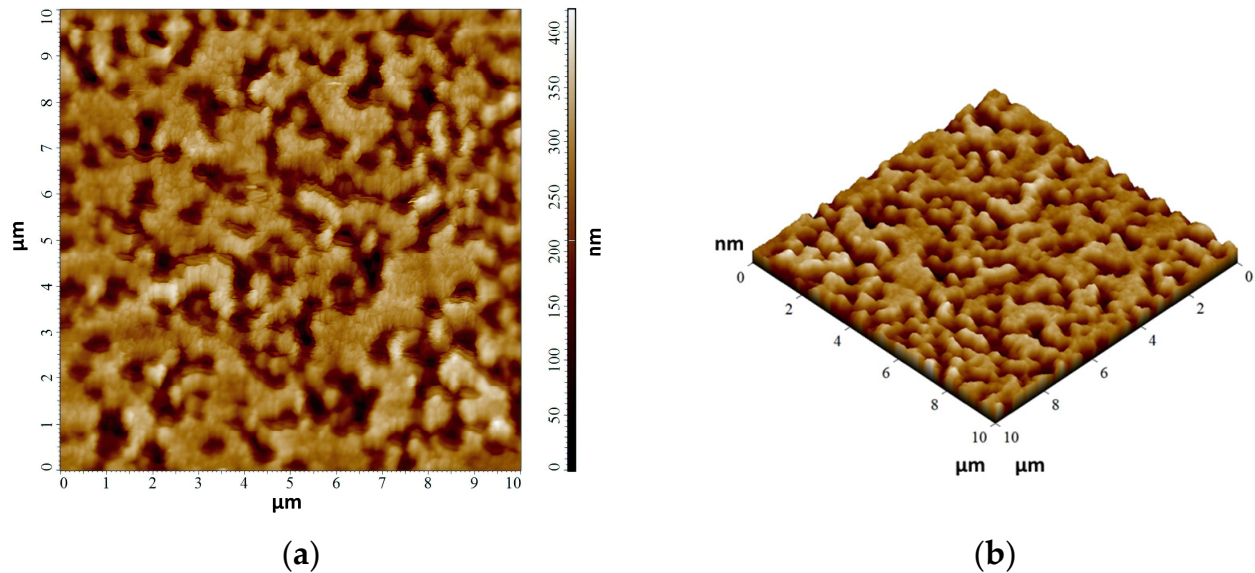


Figure 7. AFM images of the sample surface with 25 ZnO layers inside the macropore (scale $10 \times 10 \mu\text{m}$): (a) two-dimensional image; (b) three-dimensional image.

Further, to determine the structure of the surface of the samples between the micropores, the resolution of the images was increased (Figure 8).

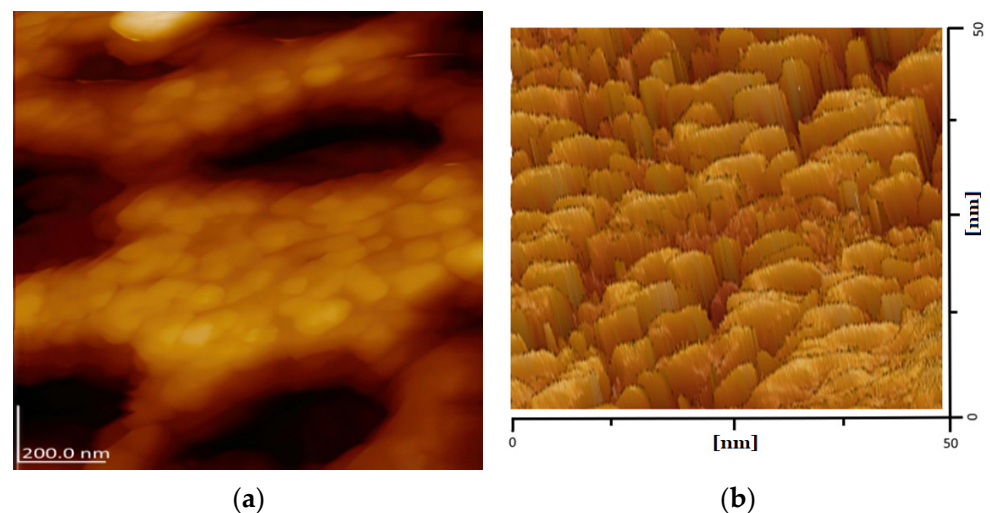


Figure 8. AFM images of the surface structure between micropores: (a) 200 nm resolution; (b) $50 \times 50 \text{ nm}$.

Figure 8a,b show that in addition to regularly spaced pores, the previously mentioned clusters of matter are clearly visible. Figure 8b shows that the clusters of matter have a similar shape and the distances between them are identical.

The following Figure 9 shows the structure of one micropore.

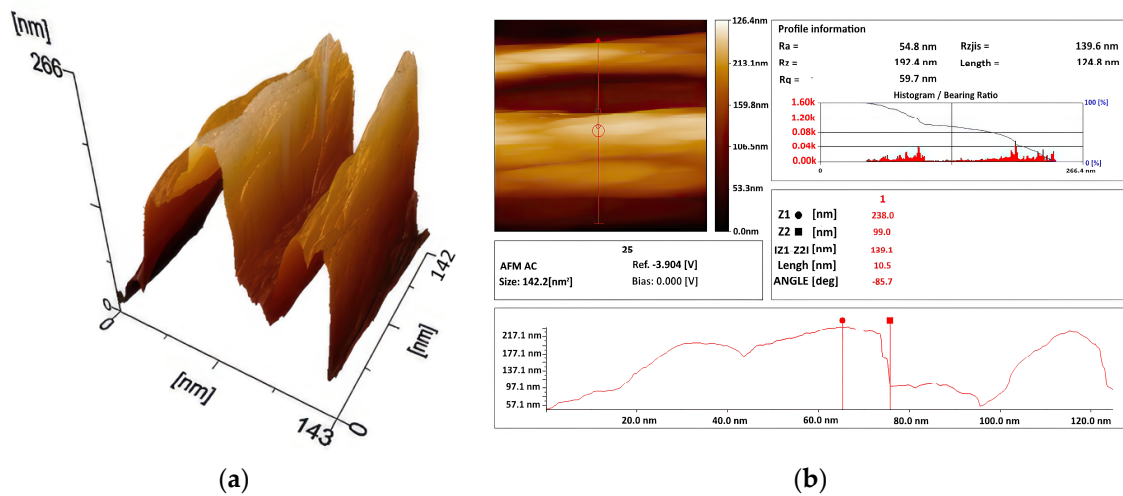


Figure 9. (a) AFM image of a single micropore; (b) analysis of micropore parameters.

The penetration of the film-forming solution occurred in different directions, which led to the formation of a developed structure inside and outside the deepening of the pores. This is important when using the developed surface as a substrate. ZnO clusters could be formed due to porous silicon substrates providing nucleation centers.

The mechanisms of formation of the nanocrystalline structure on the surface were presented in our previous article [48]. The size of the resulting ZnO structures depends on the pore size, based on the different concentrations of particles with broken bonds. Thus, estimating the thickness of ZnO is an extremely difficult task.

In the process of electrochemical etching of silicon and subsequent deposition of ZnO layers, which includes multiple annealing of samples, a substance of different phase composition is formed. XRD studies were conducted to determine the crystallinity level of the formed surface layer.

X-ray diffraction studies have revealed that only the polycrystalline phase of ZnO is observed for a sample with 25 ZnO layers. The radiographs revealed seven lines characteristic of ZnO (Figure 10). The signal from the silicon substrate is not detected due to the small angle of inclination of the X-ray beam.

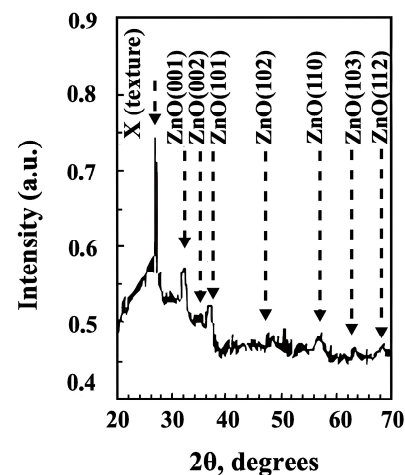


Figure 10. Radiograph of the sample with 25 layers of coating.

The average size of the zinc oxide crystallites is shown in Table 2. The XRD study for a sample with 20 layers of ZnO showed a similar result.

Table 2. Average size of ZnO crystallites for a sample with 25 layers.

Average Size of Crystallites in the Plane, nm		
ZnO (100)	ZnO (002)	ZnO (101)
15	14	13

The complexity of structures was increased through the synthesis of multilayer ZnO/SiO₂/Si. At the same time, the smaller the size of the structures, the more effective photoluminescence they have.

3.4. Photoluminescence Studies

The resulting structures contain particles of various substances. During the formation of ZnO layers on the Por-Si surface and an increase in the number of layers, the properties of the substance, in particular the light-emitting ones, change. Figure 11 shows the photoluminescence spectra for the initial sample and with the deposition of 20 and 25 coating layers (excitation wavelength is 320 nm). With a decrease in the number of ZnO layers, to less than 20, characteristic peaks of zinc oxide PL were not observed.

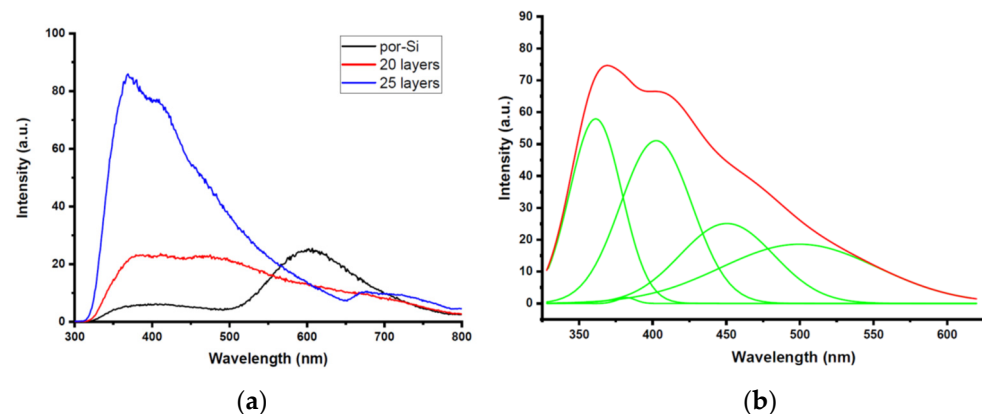


Figure 11. (a) Photoluminescence spectra of the initial sample and samples with deposited zinc oxide. (b) Photoluminescence spectrum decomposed into Gaussians for a sample with 25 layers of zinc oxide (The red line is the PL spectrum for a sample with 25 ZnO layers, the green lines are the decomposition of the spectrum into Gaussians).

The spectrum of the initial sample has a low intensity. Further, when ZnO layers are deposited, the spectrum shifts to the region of peaks typical of zinc oxide—380 nm [49] and 520 nm [28]. The complex spectrum of PL after deposition is associated with the presence of structures with different sizes. The highest intensity and the most characteristic peak for zinc oxide crystals at 380 nm is noticeable in the spectrum of a sample with 25 layers. Its nature is related to the recombination of excitons. The band at 400 nm is caused by radiative transitions near the edge of fundamental absorption. The peak of PL at ~520 nm has been observed by many researchers in ZnO nanocrystalline films. The nature of PL in this case is due to the capture of charges on oxygen vacancies [50].

At the same time, an increase of only five layers of zinc oxide significantly increases the intensity of the peak at 380 nm in comparison with a slight increase in the intensity of the peak at 520 nm. This is due to the aggregation of nanocrystals into a continuous layer on the boundaries of pores. This is confirmed by SEM studies.

The dimensions and properties of luminescent structures depend significantly on the type of substrate for the formation of ZnO layers. The following figures show the spectra of PL 25 layers of ZnO deposited under the same conditions on different substrates (Figure 12).

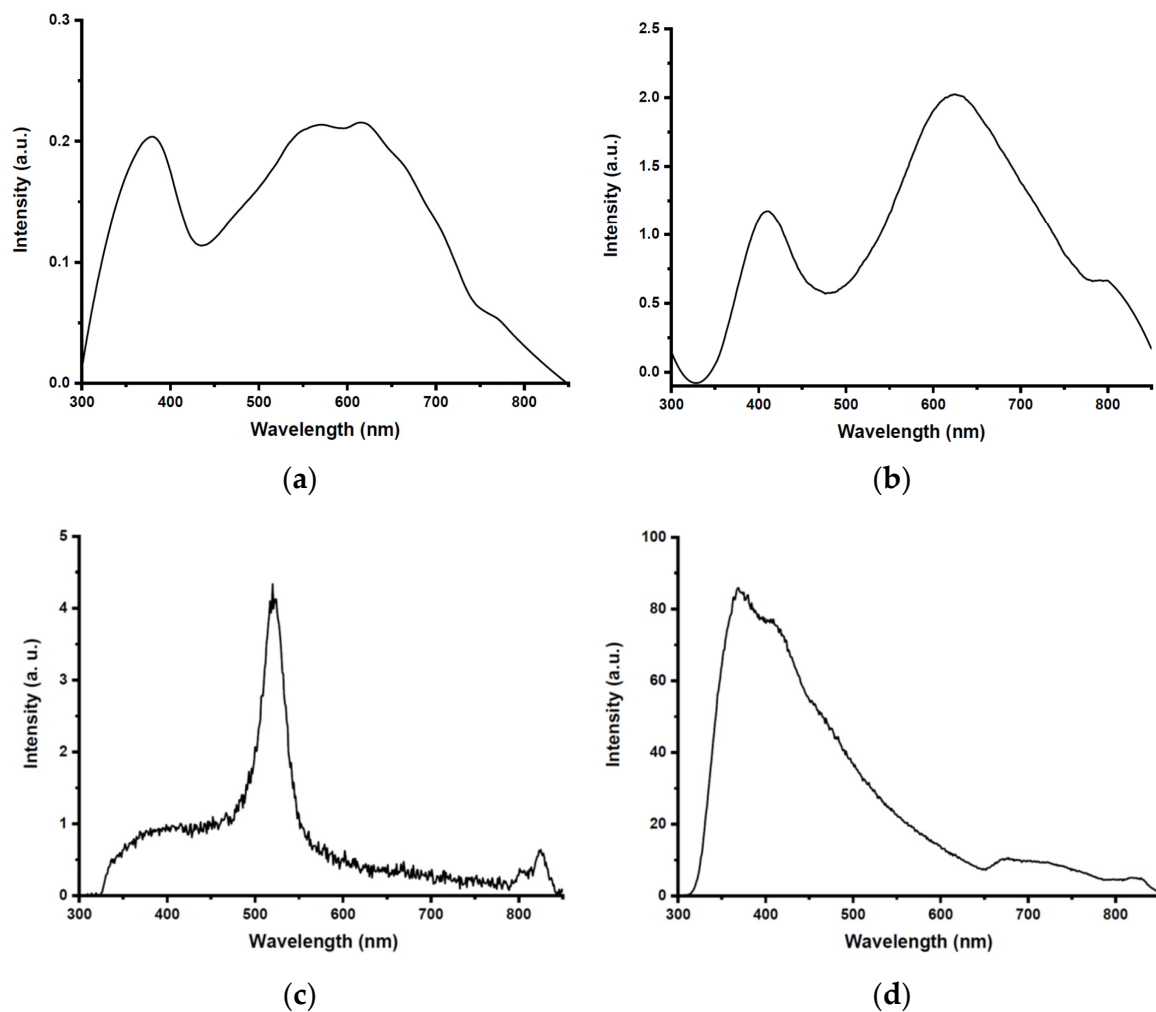


Figure 12. PL spectra for a sample with 25 coating layers deposited on various types of substrate: (a) on flat silicon; (b) on a glass substrate; (c) on porous silicon with hole conductivity; (d) on porous silicon with electron conductivity.

Studies have shown that when 25 layers of zinc oxide are deposited on different types of substrates (porous silicon, flat silicon, glass), peaks typical of zinc oxide are fixed.

The highest intensity is observed for samples with 25 layers of ZnO formed on a substrate of porous silicon with electronic conductivity. It is associated with several reasons. Firstly, there is a saturation of zinc oxide nanocrystals with electrons, because the substrate and coating have electronic conductivity. Moreover, the redistribution of electrons occurs from bulk silicon into the structure of nanocrystals, since this is an energetically advantageous direction of charge movement. Electrons are localized on the surface of nanocrystals as a result of capture on the vacancies. It is important to take into account the quantum confinement effects. They arise as a result of reducing the pore size when depositing ZnO layers, which affects the light-emitting properties [51].

The type of substrate for forming ZnO layers also affects the position of PL peaks. When comparing the spectra of samples on flat silicon and on glass, a long-wave shift of peaks is noticeable (Figure 3a,b). This occurs as a result of the formation of layers on a conductive substrate. The width of the bands at 520 nm for both types of samples is due to the contribution of several types of light-emitting structures.

In the spectrum of the sample on porous silicon of electronic conductivity, the peak near the edge of the fundamental absorption of zinc oxide (~400 nm) is most clearly manifested (Figure 3d). This is due to the saturation of the surface layers with charges and, consequently, to an increase in the intensity of this peak.

The PL for a sample on a silicon substrate of hole conductivity has the following origin. Green radiation observed at ~ 507 nm (2.43 eV) is commonly associated with the transfer of charges to deep levels in the band gap [52]. The broadband in the 330–470 nm range is probably related to the presence of tail states in the band gap. They are formed as a result of the capture of electrons from zinc oxide by holes and vacancies from silicon.

The transfer of charges is probably carried out by a jumping mechanism for oxygen vacancies. Such structures with a surface saturated with charges and their high mobility have an increased level of photosensitivity.

Previously, it was assumed that the presence of a hierarchical pore system is associated with the synthesis of a high concentration of defects with different structures and properties.

3.5. Study of the Features of the Defective Structure of the ZnO/SiO₂/Si System using EPR Method

To study the nature of the defects forming the special properties of the obtained heterostructures and to confirm a possible hypothesis, a study of ZnO/SiO₂/Si samples using the electron paramagnetic resonance method was carried out. The EPR spectra were obtained in the presence of the Mn(+2)/MgO standard, which gives six lines of super high frequency (SHF) structure, due to the interaction of unpaired electrons with the nuclear spin $I = 5/2$ of the Mn(+2) 3d⁵ ion. Special conditions were chosen for the identification of paramagnetic centers (PMCs), including changes in the microwave (MW) power and other parameters of the spectra registration. The electronic centers have spectral manifestations in the range of the third and fourth lines of the reference sample.

Figure 13a shows the spectra for the initial sample and with the ZnO coating. It is noticeable that the central part of each spectrum contains an intense signal, probably from overlapping signals from different PMCs, and its total form differs from the graph of the first derivative.

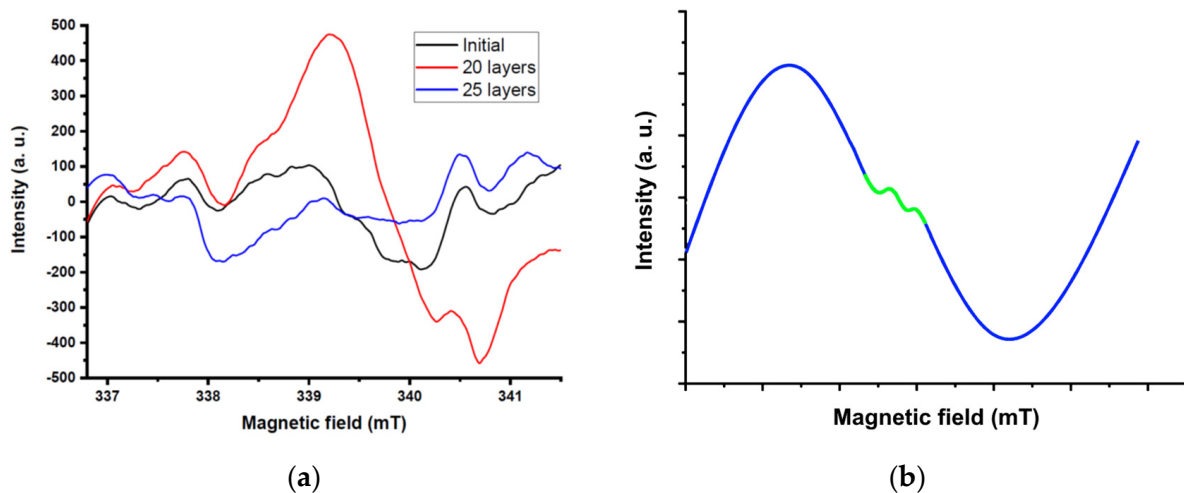


Figure 13. (a) EPR spectra of the initial sample and samples with 20 and 25 coating layers (conditions for recording spectra: $P = 10$ mW, Sweep time = 2 min, accumulation of spectra = 1, amplitude = 1.6 mT, gain factor = 800). (b) Schematic representation of the graph of the first derivative (blue line), including the manifestation of a hyperfine structure of the EPR spectrum (green line).

The formation of the defective structure at the pore boundaries occurred in several stages. The deposition of 20 layers led to the formation of individual ZnO particles, which increased the concentration of defects and the intensity of the EPR signal. This is confirmed by SEM images, which show that the structure of the pore boundaries in this sample becomes more developed. In addition, the deposition of 25 layers led to the formation of a more ordered structure, which affected the decrease in signal intensity. The SEM images for this sample show a smoother structure of the pore boundaries.

Further, to clarify the nature of PMCs, the spectra of each sample were considered separately.

For the sample with 20 coating layers, an intense spectrum of complex shape was obtained (g -factor $1.99 \div 2.00$) (Figure 14a). The difference in intensities for samples with 20 coating layers in Figures 13 and 14 are associated with different conditions for recording the spectra, which is not related to the properties of the samples. The shape of the signals in these figures is the same, which is due to the nature of the paramagnetic centers of these samples.

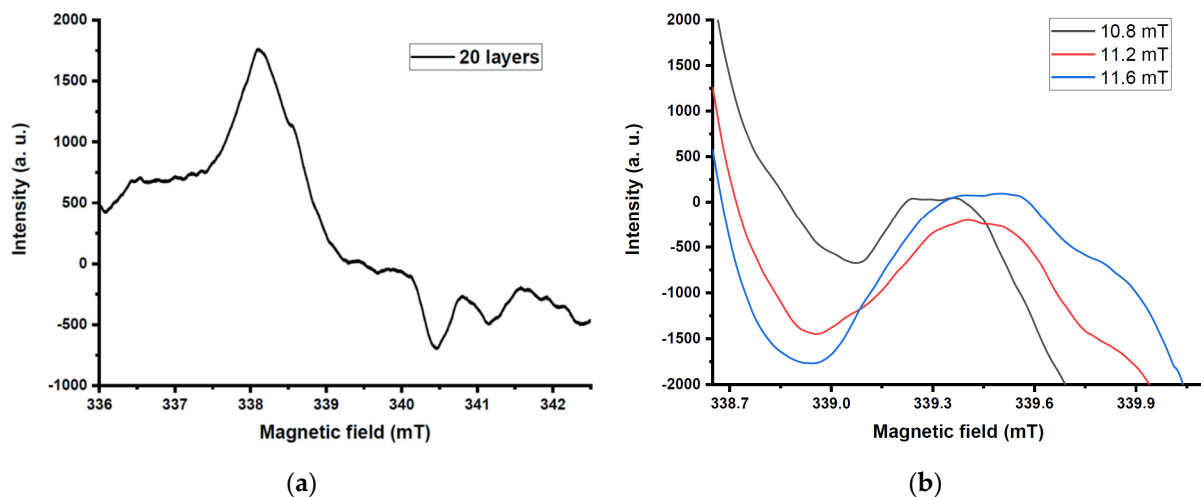


Figure 14. (a) EPR spectrum of a sample with 20 ZnO layers. (b) The range of the spectrum EPR in the area of manifestation of defects at the boundaries of the pores (20 ZnO layers).

A wide signal with $g \sim 1.99$ was observed in the center of the scanned magnetic field (~ 339 mT). It can be associated with a group of local centers at the boundaries of macropores during the formation of a ZnO coating on them (Figure 14b). The saturation of the signal starts at a relatively high microwave power (more than 10–11 mW), and the broadening of the spectrum is manifested. The relaxation time of these centers is not long because of the formation of energetically stable ZnO structures.

It should be noted that for a sample of p -type porous silicon coated with ZnO, the signal shape was close to singlet. However, it was also possible to assume the presence of anisotropy and, probably, spectral manifestations of unresolved components. Signal parameters: width 1.37 mT, g -factor value ~ 1.987 . For a sample with 25 layers, the signal intensity was increased, which is associated with a more ordered localization of PMCs [48].

For the sample with 25 layers of ZnO on Por-Si with electron conductivity, the investigation of EPR spectra was carried out with changing the parameters of registration (SHF radiation power, modulation amplitude and others). As a result, in the central part of the spectra ($338.5 \div 341.5$ mT), various spectral features can be observed (Figure 15).

Firstly, the behavior of signals in the field of electronic centers in the microwave power range (10–13.6) mW was studied. The shape of the signal (g -factor of 1.99–2.00, width ΔH_{pp} 2.32 mT) registered at a power of 10 mW is shown on Figure 16a. Further changes in the recording conditions of the signal allowed additional spectral components to be manifested (Figure 15b–d).

The shape of the signal line at $g \sim 2.00$ is shown in Figure 15 and is similar to the spectrum obtained in [53]. In that work, ZnO nanostructures were grown on films containing 10% graphene after annealing. NH_4OH , ethylene glycol and graphene oxide were used for the synthesis of films on which zinc oxide particles were formed. As it was emphasized in [53], such nanostructures have a large surface area and demonstrate high photocatalytic properties.

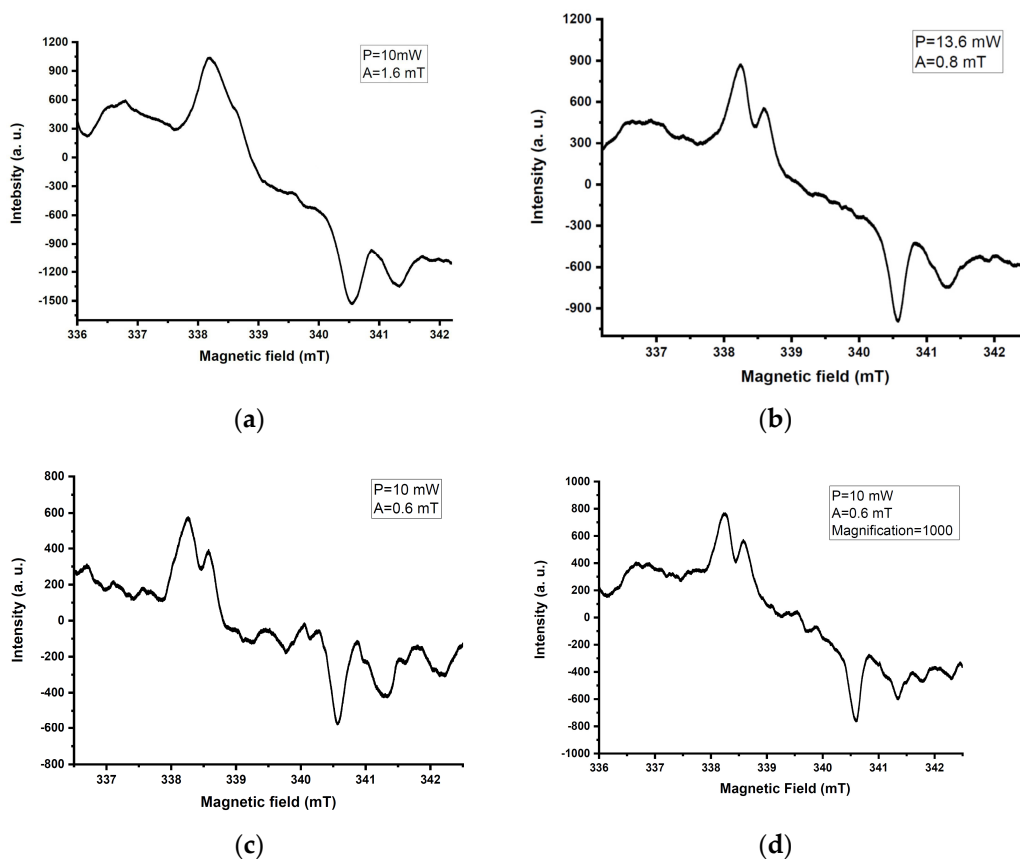


Figure 15. EPR-spectra of the sample with 25 ZnO layers at various recording parameters: (a) $P = 10$ mW, A mod 1.6 mT, Receiver Gain factor (RG)—800; (b) $P = 13.6$ mW, A mod 0.8 mT, RG—800; (c) $P = 10$ mW, A mod 0.6 mT, RG—800; (d) $P = 10$ mW, A mod 0.4 mT, RG—1000.

From comparing the stages of spectrum transformation in Figure 15b–d with the appearance of additional components, it can be concluded that the signal (g -factor is 2.2) discussed in [53] can also be decomposed into components.

Based on the fact that these developed structures are ZnO/SiO₂/Por-Si enriched with electrons, and a high concentration of vacancies have been formed on the surface, a probable way of energy transition is the capture of electrons on vacancies.

In comparison with the spectrum in Figure 15a, changes in the registration conditions of the spectra made it possible to identify signs of signals of various types of PMCs (Figure 15b–d). With an increase in power to 13.6 mW and a decrease in the modulation amplitude (A mod) to 0.8 mT, a component of a signal of lower intensity in the low-field region of the spectrum was revealed (Figure 15b). A further reduction of the A mod to 0.6 mT made it possible to reveal a complex, hyperfine structure of the spectrum in all its sections (Figure 15c). Thus, the parameters chosen for the spectra registering allowed us to distinguish the features of the signals in the spectrum and to observe increases in their intensity (Figure 15c,d). The central signal is associated with broken bonds, whereas quasi-symmetric doublets (S1/2) can probably be attributed to negatively charged vacancies formed at the boundaries of pores.

Further, the characteristics of the central part of the spectrum were studied by changing the recording parameters of the spectra and with a sequential increase in the microwave power in the range from 1 mW to 7.4 mW (Figure 16). The features of each defect—paramagnetic center—manifest themselves with a sequential change in the power of the microwave, since they have an individual saturation character.

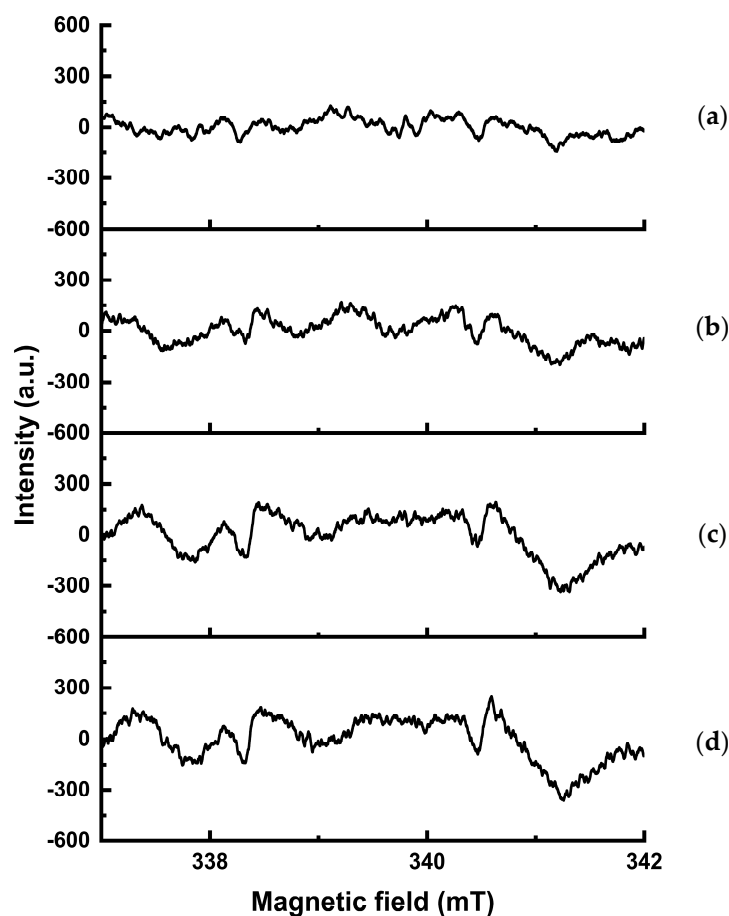


Figure 16. The EPR spectrum in the center of the magnetic field sweep in the area of manifestation of defects at the boundaries of the pores for a sample with 25 film layers: (a) $P = 1$ mW; (b) $P = 3$ mW; (c) $P = 7$ mW; (d) $P = 7.4$ mW.

Weak signals (region of g -factor ~ 2.00) of two types of paramagnetic centers connected by a dipole–dipole interaction can be distinguished in the spectra (Figure 16). This is due to the interaction of an unpaired electron with two neighbors having nuclear spin $I 1/2$. This signal is observed in a wide range of microwave power, which indicates the localization of centers in different positions in the structure of the sample. At low microwave power (1–3 mW), the presence of the signal with weak anisotropy appears in the center of the field sweep.

The changes in the intensity of the doublet signals with a change in the power of microwave radiation are different. Saturation of the central component occurred at a higher power than for the side. This allows them to be attributed to paramagnetic centers at the boundaries of pores of different sizes. The mechanism of defect formation is the capture of electrons in oxygen vacancies, similar to the formation of F-centers. A sequential change in the microwave power made it possible to separate the superimposed EPR signals due to the difference in relaxation characteristics.

The signal located in the field of doublet particles has a weak intensity. In order to manifest it in the spectrum, the sample was annealed at $t = 300$ °C in an air atmosphere for an hour (Figure 17). The melting point of zinc is 419.58 °C. Annealing at temperatures below this leads to the ordering of the structure and an increase in the level of crystallinity.

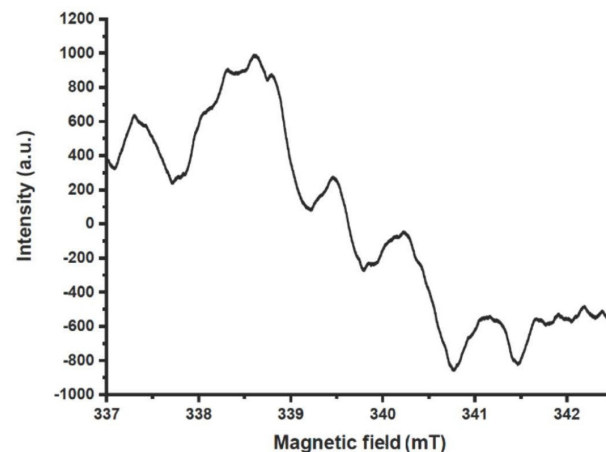


Figure 17. EPR spectrum of a sample with 25 ZnO layers after annealing at 300 °C in an air atmosphere.

The increase in signal intensity is associated with the following process. The annealing energy contributes to the diffusion of atoms by migrating to a favorable energy position. At the boundaries of zinc oxide nanoparticles, there are a lot of dangling bond–native defects. Instability of the defect region favorably affects the process of aggregation particles into clusters and an increase in grain size during annealing. Thus, the crystallinity improves during the annealing process, which leads to an increase in the intensity of the EPR signal [54].

Based on the fact that in this work the goal was to manifest the signal in the spectrum from the charge captured at the PMC, the results of the EPR spectra after annealing at other temperatures are not given.

Further research can be directed to the study of the quantum confinement effects of ZnO/Por-Si structures, in which the nano wires of the Por-Si are covered with thin layers of ZnO from above, and there are voids between these layers. There will also be a study of the relationship between the signals of duplets.

4. Conclusions

Using the method of electrochemical etching of silicon, with a decrease in the anodizing current density followed by the deposition of ZnO layers, a hierarchical structure of the sample surface was formed, including macro, micro and nanoscale objects. Deposition of ZnO layers allowed a fractal and more homogeneous surface structure to form. With an increase in the number of deposited ZnO layers from 20 to 25, the intensity of PL increases, mainly for the peak associated with the recombination of excitons, while the peak associated with the formation of ZnO nanocrystals increases with a lower intensity. This confirms the formation of an ordered structure of the surface of the samples with an increase in the number of layers, which is reflected in the SEM images. The deposition of 25 layers of ZnO on a Por-Si substrate with electronic conductivity leads to a significant (more than 40 times) increase in the intensity of PL compared to samples with other substrates. In the EPR spectra for all types of samples, multiple manifestations of the hyperfine structure caused by the capture of charges at the PMC were revealed. A decrease in the modulation amplitude and an increase in the gain coefficient of the EPR signal made it possible to effectively isolate its useful component. The intensity of the hyperfine structure of the EPR signal was significantly increased after annealing the sample at 300 °C in an air atmosphere, which is associated with an increase in the crystallinity level of the sample. The intensity of the hyperfine structure of the EPR signal was significantly increased after annealing the sample at 300 °C in an air atmosphere. This is due to an increase in the crystallinity level of the sample. The signals from ZnO structures formed at the boundaries of different-sized pores were identified based on the difference in the saturation of EPR signals.

Author Contributions: Conceptualization, T.S. and V.M.; methodology, T.S. and S.I.; software, K.A. and N.U.; validation, E.B., S.I. and E.D.; formal analysis, A.F. and K.A.; investigation, T.S., D.M. (Danatbek Murzalinov) and Y.S.; resources, S.Z. and A.F.; data curation, A.K. and S.I.; writing—original draft preparation, T.S. and D.M. (Danatbek Murzalinov); writing—review and editing, Y.S.; visualization, A.K. and E.B.; supervision, V.M. and N.U.; project administration, D.M. (Daniya Mukhamedshina) and K.M.; funding acquisition, N.U. and E.D. All authors have read and agreed to the published version of the manuscript.

Funding: This research was funded by the Science Committee of the Ministry of Science and Higher Education of the Republic of Kazakhstan (Grant No. AP09058002 «Investigation of the properties of dynamic memory based on Si₃N₄/Si and the formation of silicon nanoclusters with increased photoluminescence intensity»).

Data Availability Statement: Data are contained within the article.

Conflicts of Interest: The authors declare no conflict of interest.

References

1. Spivak, Y. Atomic-Molecular design of nanostructured materials and nanocompositions. Synthesis, technology control, properties and application. Ph.D. Thesis, Saint Petersburg Electrotechnical University “LETI”, Saint-Petersburg, Russia, 3 October 2022.
2. Lu, K. Hybrid materials—A review on co-dispersion, processing, patterning, and properties. *Int. Mater. Rev.* **2020**, *65*, 463–501. [[CrossRef](#)]
3. Shilova, O.A. Fractals, morphogenesis and triply periodic minimal surfaces in sol–gel-derived thin films. *J. Sol-Gel Sci. Technol.* **2020**, *95*, 599–608. [[CrossRef](#)]
4. Yang, X.-Y.; Chen, L.-H.; Li, Y.; Rooke, J.C.; Sanchez, C.; Su, B.-L. Hierarchically porous materials: Synthesis strategies and structure design. *Chem. Soc. Rev.* **2017**, *46*, 481–558. [[CrossRef](#)] [[PubMed](#)]
5. Mil’vidskii, M.G.; Chaldyshev, V.V. Nanometer-size atomic clusters in semiconductors—A new approach to tailoring material properties. *Semiconductors* **1998**, *32*, 457–465. [[CrossRef](#)]
6. Yan, D.; Hu, M.; Li, S.; Liang, J.; Wu, Y.; Ma, S. Electrochemical deposition of ZnO nanostructures onto porous silicon and their enhanced gas sensing to NO₂ at room temperature. *Electrochim. Acta* **2014**, *115*, 297–305. [[CrossRef](#)]
7. Razi, F.; Rahimi, F.; Irajizad, A. Fourier transform infrared spectroscopy and scanning tunneling spectroscopy of porous silicon in the presence of methanol. *Sens. Actuators B Chem.* **2008**, *132*, 40–44. [[CrossRef](#)]
8. Ozdemir, S.; Gole, J.L. A phosphine detection matrix using nanostructure modified porous silicon gas sensors. *Sens. Actuators B Chem.* **2010**, *151*, 274–280. [[CrossRef](#)]
9. Priya, V.L.; Prithivikumaran, N. Influence of Ni-Doping in ZnO Thin Films Coated on Porous Silicon Substrates and ZnO/PS Based Hetero-Junction Diodes. *Semiconductors* **2020**, *54*, 634–640. [[CrossRef](#)]
10. Banerjee, D.; Lao, J.Y.; Wang, D.Z.; Huang, J.Y.; Ren, Z.F.; Steeves, D.; Kimball, B.; Sennett, M. Large-quantity free-standing ZnO nanowires. *Appl. Phys. Lett.* **2003**, *83*, 2061–2063. [[CrossRef](#)]
11. Hahn, Y.-B. Zinc oxide nanostructures and their applications. *Korean J. Chem. Eng.* **2011**, *28*, 1797–1813. [[CrossRef](#)]
12. Frade, T.; Melo Jorge, M.E.; Gomes, A. One-dimensional ZnO nanostructured films: Effect of oxide nanoparticles. *Mater. Lett.* **2012**, *82*, 13–15. [[CrossRef](#)]
13. Wahab, R.; Ansari, S.G.; Kim, Y.-S.; Seo, H.-K.; Shin, H.-S. Room temperature synthesis of needle-shaped ZnO nanorods via sonochemical method. *Appl. Surf. Sci.* **2007**, *253*, 7622–7626. [[CrossRef](#)]
14. Kong, X.Y. Single-Crystal Nanorings Formed by Epitaxial Self-Coiling of Polar Nanobelts. *Science* **2004**, *303*, 1348–1351. [[CrossRef](#)] [[PubMed](#)]
15. Pan, Z.W. Nanobelts of Semiconducting Oxides. *Science* **2001**, *291*, 1947–1949. [[CrossRef](#)] [[PubMed](#)]
16. Wu, J.-J.; Liu, S.-C.; Wu, C.-T.; Chen, K.-H.; Chen, L.-C. Heterostructures of ZnO–Zn coaxial nanocables and ZnO nanotubes. *Appl. Phys. Lett.* **2002**, *81*, 1312–1314. [[CrossRef](#)]
17. Chen, W.J.; Liu, W.L.; Hsieh, S.H.; Tsai, T.K. Preparation of nanosized ZnO using α brass. *Appl. Surf. Sci.* **2007**, *253*, 6749–6753. [[CrossRef](#)]
18. Liu, J.; Huang, X.; Duan, J.; Ai, H.; Tu, P. A low-temperature synthesis of multiwhisker-based zinc oxide micron crystals. *Mater. Lett.* **2005**, *59*, 3710–3714. [[CrossRef](#)]
19. Huang, Y.; He, J.; Zhang, Y.; Dai, Y.; Gu, Y.; Wang, S.; Zhou, C. Morphology, structures and properties of ZnO nanobelts fabricated by Zn-powder evaporation without catalyst at lower temperature. *J. Mater. Sci.* **2006**, *41*, 3057–3062. [[CrossRef](#)]
20. Nikoobakht, B.; Wang, X.; Herzing, A.; Shi, J. Scalable synthesis and device integration of self-registered one-dimensional zinc oxide nanostructures and related materials. *Chem. Soc. Rev.* **2013**, *42*, 342–365. [[CrossRef](#)]
21. Tien, L.C.; Pearton, S.J.; Norton, D.P.; Ren, F. Synthesis and microstructure of vertically aligned ZnO nanowires grown by high-pressure-assisted pulsed-laser deposition. *J. Mater. Sci.* **2008**, *43*, 6925–6932. [[CrossRef](#)]
22. Cui, J. Zinc oxide nanowires. *Mater. Charact.* **2012**, *64*, 43–52. [[CrossRef](#)]

23. Chiu, W.S.; Khiew, P.S.; Cloke, M.; Isa, D.; Tan, T.K.; Radiman, S.; Abd-Shukor, R.; Abd Hamid, M.A.; Huang, N.M.; Chia, C.H.; et al. Photocatalytic study of two-dimensional ZnO nanopellets in the decomposition of methylene blue. *Chem. Eng. J.* **2010**, *158*, 345–352. [[CrossRef](#)]
24. José-Yacamán, M.; Gutierrez-Wing, C.; Miki, M.; Yang, D.-Q.; Piyakis, K.N.; Sacher, E. Surface Diffusion and Coalescence of Mobile Metal Nanoparticles. *J. Phys. Chem. B* **2005**, *109*, 9703–9711. [[CrossRef](#)] [[PubMed](#)]
25. Polshettiwar, V.; Baruwati, B.; Varma, R.S. Self-Assembly of Metal Oxides into Three-Dimensional Nanostructures: Synthesis and Application in Catalysis. *ACS Nano* **2009**, *3*, 728–736. [[CrossRef](#)] [[PubMed](#)]
26. Xie, Q.; Dai, Z.; Liang, J.; Xu, L.; Yu, W.; Qian, Y. Synthesis of ZnO three-dimensional architectures and their optical properties. *Solid State Commun.* **2005**, *136*, 304–307. [[CrossRef](#)]
27. Liu, J.; Huang, X.; Li, Y.; Sulieman, K.M.; Sun, F.; He, X. Selective growth and properties of zinc oxide nanostructures. *Scr. Mater.* **2006**, *55*, 795–798. [[CrossRef](#)]
28. Bitenc, M.; Crnjak Orel, Z. Synthesis and characterization of crystalline hexagonal bipods of zinc oxide. *Mater. Res. Bull.* **2009**, *44*, 381–387. [[CrossRef](#)]
29. Kołodziejczak-Radzimska, A.; Jesionowski, T. Zinc Oxide—From Synthesis to Application: A Review. *Materials* **2014**, *7*, 2833–2881. [[CrossRef](#)]
30. Karthik TV, K.; Martinez, L.; Agarwal, V. Porous silicon ZnO/SnO₂ structures for CO₂ detection. *J. Alloys Compd.* **2018**, *731*, 853–863. [[CrossRef](#)]
31. Vlasenko, L.S. Magnetic Resonance Studies of Intrinsic Defects in ZnO: Oxygen Vacancy. *Appl. Magn. Reson.* **2010**, *39*, 103–111. [[CrossRef](#)]
32. Zhapakov, R.; Begunov, M.; Serejavina, T.; Murzalinov, D.; Serikkanov, A.; Dmitriyeva, E.; Zhantuarov, S.; Ibraimova, S. Defect Formation of Light-Emitting Particles during the Synthesis of a Hierarchical Porous Surface of ZnO/SiO₂/Si Structures. *Eng. Proc.* **2023**, *37*, 43. [[CrossRef](#)]
33. Marin, O.; Grinblat, G.; Gennaro, A.M.; Tirado, M.; Koropecski, R.R.; Comedi, D. On the origin of white photoluminescence from ZnO nanocones/porous silicon heterostructures at room temperature. *Superlattices Microstruct.* **2015**, *79*, 29–37. [[CrossRef](#)]
34. Martínez, L.; García-Salgado, G.; Morales-Morales, F.; Campillo, B.; Hernández, A.G.; Karthik TV, K.; Jimenez-Vivanco, M.R.; Campos-Álvarez, J. ZnO Films Incorporation Study on Macroporous Silicon Structure. *Materials* **2021**, *14*, 3697. [[CrossRef](#)] [[PubMed](#)]
35. Li, Y.; Xu, L.; Li, X.; Shen, X.; Wang, A. Effect of aging time of ZnO sol on the structural and optical properties of ZnO thin films prepared by sol–gel method. *Appl. Surf. Sci.* **2010**, *256*, 4543–4547. [[CrossRef](#)]
36. Bedia, A.; Bedia, F.Z.; Aillerie, M.; Maloufi, N.; Benyoucef, B. Influence of the Thickness on Optical Properties of Sprayed ZnO Hole-blocking Layers Dedicated to Inverted Organic Solar Cells. *Energy Procedia* **2014**, *50*, 603–609. [[CrossRef](#)]
37. Prabakaran, R.; Peres, M.; Monteiro, T.; Fortunato, E.; Martins, R.; Ferreira, I. The effects of ZnO coating on the photoluminescence properties of porous silicon for the advanced optoelectronic devices. *J. Non-Cryst. Solids* **2008**, *354*, 2181–2185. [[CrossRef](#)]
38. Spivak, Y.M.; Gagarina, A.Y.; Portnova, M.O.; Zaikina, A.V.; Moshnikov, V.A. One-step electrochemical synthesis of Ag/por-Si composite from monocrystalline Si. *J. Phys. Conf. Ser.* **2020**, *1697*, 012126. [[CrossRef](#)]
39. Korotcenkov, G.; Cho, B.K. Silicon Porosification: State of the Art. *Crit. Rev. Solid State Mater. Sci.* **2010**, *35*, 153–260. [[CrossRef](#)]
40. Snow, P.A.; Squire, E.K.; Russell PS, J.; Canham, L.T. Vapor sensing using the optical properties of porous silicon Bragg mirrors. *J. Appl. Phys.* **1999**, *86*, 1781–1784. [[CrossRef](#)]
41. Wang, G.; Gu, Y.; Zhao, L.; Xuan, J.; Zeng, G.; Tang, Z.; Sun, Y. Experimental and numerical investigation of fractal-tree-like heat exchanger manufactured by 3D printing. *Chem. Eng. Sci.* **2018**, *195*, 250–261. [[CrossRef](#)]
42. Mwema, F.M.; Akinlabi, E.T.; Oladijo, O.P.; Fatoba, O.S.; Akinlabi, S.A.; Tălu, S. Advances in manufacturing analysis: Fractal theory in modern manufacturing. In *Modern Manufacturing Processes*; Woodhead Publishing: Sawston, UK, 2019; pp. 13–39. [[CrossRef](#)]
43. Hosseinabadi, S.; Shirazi, M. Contour loop analysis of multi-affine nanostructure AZO rough surfaces. *Surface Topography: Metrol. Prop.* **2019**, *7*, 035007. [[CrossRef](#)]
44. Zhou, F.; Huang, Y.M. Fractal microstructures of light-emitting porous silicon films. *Appl. Surf. Sci.* **2007**, *253*, 4507–4511. [[CrossRef](#)]
45. Ghosh, K.; Pandey, R.K. Assessment of fractal and multifractal features of sol-gel spin coated ZnO thin film surface. *Mater. Res. Express* **2019**, *6*, 086454. [[CrossRef](#)]
46. Annadhasan, A. Methods of fractal dimension computation. *Int. J. Comput. Sci. Inf. Technol. Secur.* **2012**, *2*, 166–169.
47. Bobkov, A.; Kononova (Grachova), I.; Moshnikov, V. *Materials Science of Micro- and Nanosystems. Hierarchical Structures*; Saint Petersburg Electrotechnical University “LETI”: Saint-Petersburg, Russia, 2017.
48. Murzalinov, D.; Kemelbekova, A.; Serejavina, T.; Spivak, Y.; Serikkanov, A.; Shongalova, A.; Zhantuarov, S.; Moshnikov, V.; Mukhamedshina, D. Self-Organization Effects of Thin ZnO Layers on the Surface of Porous Silicon by Formation of Energetically Stable Nanostructures. *Materials* **2023**, *16*, 838. [[CrossRef](#)] [[PubMed](#)]
49. Hourdakis, E.; Bardakas, A.; Segkos, A.; Tsilivaki, S.; Gardelis, S.; Tsamis, C. Tunable and white light photoluminescence from ZnO on porous Si with the addition of carbon quantum dots. *Nanotechnology* **2023**, *34*, 455202. [[CrossRef](#)] [[PubMed](#)]
50. Rodnyi, P.A.; Chernenko, K.A.; Venevtsev, I.D. Mechanisms of ZnO Luminescence in the Visible Spectral Region. *Opt. Spectrosc.* **2016**, *125*, 372–378. [[CrossRef](#)]

51. Husairi, F.S.; Eswar, K.A.; Guliling, M.; Khusaimi, Z.; Rusop, M.; Abdullah, S. Porosity and thickness effect of porous silicon layer on photoluminescence spectra. In Proceedings of the 8th International Conference on Nanoscience and Nanotechnology, Selangor, Malaysia, 24–27 February 2017. [[CrossRef](#)]
52. Salem, J.K.; Hammad, T.M.; Harrison, R.R. Synthesis, structural and optical properties of Ni-doped ZnO micro-spheres. *J. Mater. Sci. Mater. Electron.* **2012**, *24*, 1670–1676. [[CrossRef](#)]
53. Ahmed, G.; Hanif, M.; Mahmood, K.; Yao, R.; Ning, H.; Jiao, D.; Wu, M.; Khan, J.; Liu, Z. Lattice defects of ZnO and hybrids with GO: Characterization, EPR and optoelectronic properties. *AIP Adv.* **2018**, *8*, 025218. [[CrossRef](#)]
54. Mamat, M.H.; Sahdan, M.Z.; Amizam, S.; Rafaie, H.A.; Khusaimi, Z.; Ahmed, A.Z.; Abdullah, S.; Rusop, M. The effect of annealing temperatures on zinc oxide thin films properties for electronic devices application. In Proceedings of the 2008 IEEE International Conference on Semiconductor Electronic, Johor Bahru, Malaysia, 25–27 November 2008. [[CrossRef](#)]

Disclaimer/Publisher's Note: The statements, opinions and data contained in all publications are solely those of the individual author(s) and contributor(s) and not of MDPI and/or the editor(s). MDPI and/or the editor(s) disclaim responsibility for any injury to people or property resulting from any ideas, methods, instructions or products referred to in the content.